PCCP

ROYAL SOCIETY OF CHEMISTRY

PAPER

View Article Online
View Journal | View Issue

Cite this: *Phys. Chem. Chem. Phys.*, 2026, **28**, 7136

Structure-making solvation of ferulic acid across protic and aprotic solvents: viscosity experiments, simulations, and implications for antioxidant function

Renato Tomaš, [a] Olivera Politeo, [a] Milan Vraneš, [b] Moez Guettari, [c] Safija Herenda [d] and Martina Požar *[e]

Solvent structure-making is an important feature of molecular organization in liquids as it shapes thermodynamic, dynamic and reactive properties. In this paper, we combine experimental and computational approaches to elucidate the structure-making behaviour of *trans*-4-hydroxy-3-methoxycinnamic acid (ferulic acid, FA) in a series of solvents: the protic alcohols methanol, ethanol, and 2-propanol, and the aprotic solvents tetrahydrofuran (THF) and dimethyl sulfoxide (DMSO). Precise viscometric measurements over 11 temperatures in the molality range from ~0.01 to ~0.5 mol kg^{-1} reveal that FA acts as a structure-maker across all solutions. Molecular dynamics simulations complement these findings, revealing marked cross-species correlations and mixed clusters in protic solvents. Hydrogen-bond analysis highlights the long lifetimes of cross-species hydrogen bonds, underscoring the dual donor–acceptor capacity of FA. The insights from experiments and simulations provide a molecular foundation for understanding how solute-induced structure-making by ferulic acid influences solvent organization, and ultimately, properties such as viscosity and antioxidant performance.

Received 4th December 2025,
Accepted 13th February 2026

DOI: 10.1039/d5cp04726a

rsc.li/pccp

1. Introduction

trans-Ferulic acid or simple ferulic acid (*trans*-4-hydroxy-3-methoxycinnamic acid, FA) (Fig. 1) is an antioxidant or bioactive compound belonging to a group of chemicals called hydroxycinnamic acids.[1] It is found in the cells of plants *Ferula asafoetida* L.[2] and *Ligusticum chuanxiong*,[3] but also in more common dietary staples such as grapes, coffee, tomatoes, apples, and spinach.[4] It is also found in red wine in concentrations ranging from 2×10^{-3} to 1 mg/100 mL.[5] FA has been widely used in Chinese medicine due to its positive effects against oxidative stress, inflammation, vascular endothelial injury, fibrosis, apoptosis and platelet aggregation.[6] These beneficial properties have spurred the use of FA in skincare products, such as sunscreens[7] and anti-aging creams.[8] Additionally, there are studies on the therapeutic effects of FA against cancer,[9,10] diabetes,[11] cardiovascular[12] and neurodegenerative[13,14] diseases.

Despite its significant antioxidant activity and broad bioactivity profile, the widespread usage of FA in biological and pharmaceutical systems is hampered by two factors. The first factor is its limited ability to penetrate the soluble lipid bilayer and enter the cell,[15] due to the molecule's short alkane chain and large polarity. However, this problem was remedied by chemical modification strategies, such as esterification with fatty alcohols, which improved the antibacterial activity of FA as per the work of Song and coworkers.[15] The second factor, which is also more pertinent for this work, is the poor solubility of FA

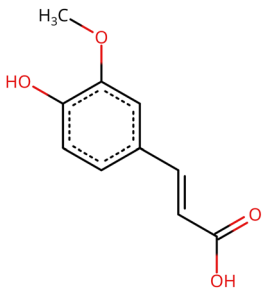

Fig. 1 *trans*-Ferulic acid (FA).

[a] *Faculty of Chemistry and Technology, University of Split, Ruđera Boškovića 35, HR-21000 Split, Croatia*
[b] *Faculty of Sciences, University of Novi Sad, Trg Dositeja Obradovića 3, 21000 Novi Sad, Serbia*
[c] *Materials and Fluids Laboratory, Preparatory Institute for Engineering studies of Tunis, University of Tunis, Tunisia*
[d] *Faculty of Science, University of Sarajevo, Zmaja od Bosne 35, 71 000 Sarajevo, Bosnia and Herzegovina*
[e] *Faculty of Science, University of Split, Ruđera Boškovića 33, HR-21000 Split, Croatia. E-mail: marpoz@pmfst.hr*

in water. As shown in the work of Shakeel *et al.*,[16] FA displays a solubility of 4.89×10^{-5} mole fraction in water under ambient conditions, which increases at higher pH due to deprotonation. In contrast, FA is much more soluble in various organic solvents such as alcohols, glycols and polar aprotic solvents such as dimethyl sulfoxide, with mole fraction solubilities up to about 0.1 at 298.2 K for certain solutes,[16] which tend to increase with an increase in temperature. However, the most intriguing solvent featured in the paper of Shakeel *et al.*[16] is ethanol. Ethanol stands out as the only medium suitable for human consumption, which hints at its potential role as a carrier for FA, thus playing a role in antioxidant applications.

From a molecular perspective, the solvation of ferulic acid ought to be strongly influenced by solvent properties. Protic solvents such as methanol, ethanol and 2-propanol contain O–H groups that can donate hydrogen bonds and efficiently stabilize charged or strongly polar species. In contrast, polar aprotic solvents such as dimethyl sulfoxide (DMSO) and tetrahydrofuran (THF) lack O–H or N–H groups, so they cannot form hydrogen bonds with themselves, although they have large dipole moments and act as good hydrogen-bond acceptors. These differences in hydrogen-bonding ability and polarity are expected to affect the solvation of ferulic acid and its structure-making or structure-breaking effect in solution, which is in turn reflected in transport properties such as viscosity. In this work, we showcase a systematic study of ferulic acid in selected polar protic (methanol, ethanol, 2-propanol) and polar aprotic (THF, DMSO) solvents over a wide temperature range. The paper combines very precise viscometric experiments with molecular dynamics simulations, rounded out with antioxidant assays on FA in selected solvents.

In the first part of this paper we report precise density and dynamic viscosity data. From viscosity data in investigated systems for FA in different solvents at 11 temperatures (from 273.15 to 323.15 K in steps of 5 K), and in the molality range from $\sim$0.01 to $\sim$0.5 mol kg^{-1}, the relative viscosity data η_r have been analyzed and interpreted in terms of the Jones–Dole equation. Viscosity *B*-coefficients were determined and discussed in terms of FA–solvent interactions. Based on the available literature, experimental data for investigating binary systems (FA + S) at various temperatures have not yet been reported. Only a few existing papers concerning FA in various solvents were found. Chen *et al.*[17] investigated the interaction of ferulic acid in aqueous ethanol/propan-1-ol solutions using volumetric, viscometric and refractive index approaches, demonstrating the presence of strong solute–solvent interactions in the studied aqueous alcohol systems. The authors found that FA acts as a structure-maker solute in the investigated systems. Sahin *et al.*[18] measured the density and speed of sound for *p*-coumaric acid, caffeic acid and ferulic acid in methanol at different temperatures, determining the solute–solvent interactions. Villanueva-Bermejo *et al.*[19] determined the solubility of bioactive substances (FA and caffeine) in ethyl lactate + water mixtures and concluded that the acid solubility in the respective mixed solvents was considerably higher than in either pure ethyl lactate or water.

The viscosity experiments were supplemented with viscosity calculations, structural properties and hydrogen bond dynamics from molecular dynamics (MD) simulations in order to gain a microscopic insight into the interactions that shape the observed macroscopic behavior. To the best of our knowledge, this is the first MD simulation of FA in the abovementioned five solvents. However, in recent years, there have been several MD simulation studies on FA in two different contexts: the role of solvent in solvation and nucleation, and the interaction of FA (or its derivatives) with biomacromolecular targets. The former category is rather scarce, with the work of Lin *et al.* who combined MSZW/solubility experiments with MD to probe the solvent–solute hydrogen bonding and self-association trends in mixtures of FA with organic solvents.[20] The latter category, which examines how FA (or closely related esters/derivatives) bind to proteins and enzymes, is better represented. Chen *et al.* investigated the complexes FA formed with ovalbumin through spectroscopy, MD and docking,[21] while Amshumala and coworkers studied the different conformers of the complex between the transcription factor Nrf2 and ferulic acid, also through MD simulations and spectroscopy.[22] Yang *et al.* reported RMSD/RMSF and hydrogen-bond counts for FA and FA methyl ester complexes with human serum albumin and lysozyme.[23] MD simulations of FA derivatives extend to larger ligands and enzyme targets (for example, SARS-CoV-2 Mpro), where MD results of RMSD, radius of gyration and hydrogen-bonding were used to judge complex stability.[24]

We conclude the paper with the antioxidant efficacy of FA in selected solvents, which was additionally tested in this work and discuss the implications of the structure-making properties of FA on the results of antioxidant assays. Regulatory bodies and journals in the food industry often expect the use of multiple antioxidant assays due to the fact that different methods have different mechanisms of action,[25,26] so using one assay alone is considered insufficient for a reliable antioxidant profile.[27] Two different antioxidant capacity assays, DPPH and FRAP, were employed in this study. DPPH measures free radical scavenging, while FRAP measures electron-donating capacity,[28] and in tandem, they are used for general antioxidant screening, enabling a more reliable and comprehensive evaluation of the sample's antioxidant capacity.

The remainder of the paper is structured as follows. Section 2 describes the preparation of samples, the viscosimetry experiment protocol, the determination of the antioxidant capacity and the simulation protocol together with calculation details. In Section 3 we showcase, analyze and discuss our results, while Section 4 closes the presentation of this work.

2. Experimental section

2.1 Chemicals

Solvents MeOH (Sigma-Aldrich, p.a., USA), absolute EtOH (GramMol, p.a., Croatia), 2-PrOH (GramMol, p.a., Croatia), DMSO (Sigma-Aldrich, p.a., USA) and THF (Emplura, p.a., Germany) were used without further purification. *trans*-

Ferulic acid (FA) (Sigma-Aldrich, USA, purity >99.9%) was used as received. All solutions were prepared gravimetrically by weighing appropriate amounts of FA and solvent on an analytical balance (Sartorius RC 210D) with an uncertainty of $\pm 1 \times 10^{-5}$ g. Based on literature solubility data at 318 K[16] and preliminary tests at room temperature, homogeneous solutions with FA molality up to about 1 mol kg^{-1} could be prepared in all solvents. At higher FA contents, visible crystallization of FA occurred after standing for 24 h at room temperature. Therefore, measurements were restricted to the molality range up to about 0.5 mol kg^{-1}, where no crystallization was observed during the experimental time scale.

2.2 Apparatus and procedure for density and viscosity measurements

Densities (ρ) of FA solutions in different solvents at various temperatures were measured using an Anton Paar DMA 4500 M densimeter (Austria) equipped with a built-in Peltier thermostat for temperature control ($\pm$0.01 K). Before each series of measurements, the instrument was calibrated at atmospheric pressure (p = 101.0 kPa) using triple-distilled water and dry air over the investigated temperature range. Further details on the density measurements are given elsewhere.[29–31]

Dynamic viscosities (η) for the same solutions were measured using a fully automated Anton Paar SVM 3001 kinematic viscometer (crafted in Austria). The instrument is equipped with a thermostated measuring cell, whose temperature is controlled by a cascade Peltier element, with a temperature repeatability of 0.005 K. The repeatability of viscosity measurements was $\pm$0.1%, and the reproducibility was 0.35%. Prior to measurements, the viscometer was calibrated with a certified viscosity standard (Anton Paar S3 (L), 3.7/2.3/0.9 mPa s) according to ASTM D2162. Kinematic viscosities were automatically calculated from the measured dynamic viscosities and densities.

The total volume of the sample used for both measurements was about 1 mL. The densimeter and viscometer already have an incorporated moisture adsorbent.

Molar concentrations (c) given in Tables S1–S5 (SI) were obtained from molality (m) and density data, using the standard relationship $c = 1000\rho m/(1000 + mM)$, where M is the molar mass of FA.

2.3 Determination of antioxidant capacity

The antioxidant capacity of ferulic acid (FA) solutions was determined using two assays: the DPPH radical scavenging method and the reducing capacity (FRAP) method. Measurements were performed using Sunrise microtiter plate readers (Tecan GmbH, Austria).

The ability of solutions to neutralize free DPPH radicals was assessed using the method described by Brand-Williams *et al.*[32] DPPH$^{\bullet}$ has been extensively employed to evaluate the free radical scavenging capacity of samples. The results were expressed as IC_{50} values, defined as the FA concentration required to inhibit 50% of DPPH radicals. A lower IC_{50} value indicates a stronger antioxidant potential of the sample. The radical scavenging activity of the tested extracts was quantified using the formula:

$$\%\ \text{inhibition} = \frac{A_0 - A_{\text{sample}}}{A_0} \times 100\% \quad (1)$$

where A_0 represents the initial absorbance of the DPPH ethanol solution at 517 nm, and A_{sample} corresponds to the absorbance of the sample measured after 60 minutes. The FRAP assay was conducted following the method described by Benzie and Strain.[33] The reducing power of the samples was determined by comparing their reaction signal to that of a Fe^{2+} ion solution with a known concentration and expressed as Fe^{2+} mmol L^{-1}. The tested concentration of FA solutions was 0.5 mM.

2.4 Simulation details

Molecular dynamics (MD) simulations were performed using the program package GROMACS 2023.3.[34] The simulated systems correspond to the experimental ones: methanol – FA, ethanol – FA, 2-propanol – FA, DMSO – FA and THF – FA. For all systems, the simulations were performed at 3 temperatures: T = 278 K, T = 298 K and T = 318 K. For each temperature, we simulated 2 mole fractions of FA in a particular solvent: the highest and the intermediate mole fraction of FA, corresponding to the systems prepared for viscosity measurements.

To simulate methanol, ethanol and 2-propanol we chose the OPLS-UA force field for alcohols.[35] Likewise, the OPLS-UA models were used for DMSO and THF,[36] while FA was constructed with the OPLS-AA approach.[37]

The starting configurations for each system consisted of 2048 molecules distributed randomly in a cubic box, courtesy of the Packmol program.[38] The simulation protocol was the same for each system. Each box first went through energy minimization, followed by 5 ns of equilibration and 5 ns of production at the desired temperature. These simulations were done in the NpT ensemble at p = 1 bar and T = 278 K, 298 K and 318 K. The temperatures were kept constant with the v-rescale thermostat[39] which had a time constant of 0.2 ps. The pressure was maintained with the Parrinello–Rahman barostat,[40,41] which had a time constant of 2 ps. The integration algorithm of choice was the leap-frog algorithm,[42] with a time-step of 2 fs. The short-range interactions were calculated within the 1.5 nm cut-off radius, whereas the long-range electrostatics were calculated using the PME method.[43] The constraints were handled with the LINCS algorithm.[44] During the production run, 2000 configurations were collected to extract the structural properties, hydrogen bonding properties and the viscosities.

We have calculated several structural properties from the simulations. The pair correlation function $g(r)$ describes the probability of finding a particle at a distance r from a reference particle:[45]

$$g(r) = \frac{1}{4\pi r^2 \rho N}\left\langle \sum_{i=1}^{N}\sum_{j\neq i}\delta\left(r - r_{ij}\right)\right\rangle \quad (2)$$

where ρ is the average number density and r_{ij} is the distance between particles i and j.

The pair correlation function is the basis for calculating the coordination number $n(r)$, which gives the average number of particles within a distance r from a reference particle:

$$n(r) = 4\pi\rho\int_0^r g_{ij}(r)r^2\mathrm{d}r \quad (3)$$

where once again, ρ is the average number density.

The cluster probability distributions $P(s)$ were calculated within the Gromacs module gmx clustsize, which identifies molecular clusters based on a distance criterion, with r_c being the cutoff distance which is usually taken as the first minimum in the $g(r)$. The cutoff values for all the O sites were taken as r_c = 0.35 nm. The histograms of cluster occurrences computed over the entire trajectory were used to find the time-averaged probability $P(s)$ of finding a cluster of a size s.

The hydrogen bond autocorrelation functions and subsequent lifetimes were calculated following Luzar and Chandler[46,47] as implemented in the Gromacs gmx hbond module. The hydrogen-bond autocorrelation function $C(t)$ describes the time-dependent persistence of hydrogen bonds. It measures the conditional probability that a hydrogen bond present at time 0 remains continuously intact at time t:

$$C(t) = \frac{\langle h(0)h(t)\rangle}{\langle h\rangle} \quad (4)$$

where $h(t)$ = 1 if a specific donor–acceptor pair is hydrogen-bonded at time t (according to the geometric criterion where $r_{DA} < r_c$ and $\theta_{HDA} < \theta_c$), and $h(t)$ = 0 otherwise. The average $\langle h\rangle$ normalizes the function such that $C(0)$ = 1.

The continuous hydrogen-bond lifetime τ_{HB}^{cont} is the average duration of time over which a hydrogen bond remains continuously intact. In the Luzar–Chandler formalism,[46,47] it is obtained by integrating the autocorrelation function $C(t)$:

$$\tau_{HB}^{cont} = \int_0^\infty C(t)\mathrm{d}t \quad (5)$$

The intermittent hydrogen-bond correlation function $H(t)$ describes the probability that a hydrogen bond present at time t = 0 exists at a later time t, regardless of any intermittent breaking and reforming events, and is defined as:

$$H(t) = \frac{\langle h(0)h(t)\rangle}{\langle h\rangle} \quad (6)$$

where $h(t)$ = 1 if a given donor–acceptor pair satisfies the geometric hydrogen-bond criteria at time t, and $h(t)$ = 0 otherwise.

The corresponding intermittent hydrogen-bond lifetime τ_{HB}^{int} is obtained by time integration of $H(t)$:

$$\tau_{HB}^{int} = \int_0^\infty H(t)\mathrm{d}t \quad (7)$$

The shear viscosity η in our simulations was calculated *via* the Einstein formula:

$$\eta = \frac{1}{2}\frac{V}{k_B T}\lim_{t\to\infty}\frac{\mathrm{d}}{\mathrm{d}t}\left\langle\left(\int_{t_0}^{t_0+t}P_{xz}(t')\mathrm{d}t'\right)\right\rangle_{t_0} \quad (8)$$

where V is the volume of the system, k_B is the Boltzmann constant, T is the temperature of the system and P_{xz} is an off-diagonal component of the pressure tensor (the xz component), and $\langle\cdots\rangle_{t_0}$ is the average over time.

3. Results and discussion

3.1 Viscosity *B*-coefficient of ferulic acid in near solvents

The measured density and viscosity data for solutions of different concentrations of FA in all investigated solvents at various temperatures are given in Tables S1–S5 in the SI, as the mean of three independent measurements. Furthermore, our densities and viscosities for used solvents (c_{FA} = 0 mol dm^{-3}) are in very good agreement with data available in the literature over the entire temperature range (see Fig. S1 in the SI). The overall consistency indicates that the present density and viscosity data provide a reliable basis for further analysis and interpretation.

In Fig. 2, a comparison between the viscosities for the five investigated systems in this work at a temperature T of 298.15 K are graphically presented. At the same concentration, the lowest value is for FA in THF, and the highest is for FA in 2-PrOH.

Our experimentally determined new values of viscosities, $\eta(m, T)$, for FA in different solvents were used for calculating viscosity B-coefficients and their temperature dependence. It should be noted that FA behaves as a weak electrolyte in a polar solvent (partial dissociation into ions), and the viscosity can be analyzed by using the following relationship:

$$\eta_r - 1 = Bc \quad (9)$$

where η_r is the relative viscosity and corresponds to $\eta_r = \eta/\eta_0$, and c denotes the molarity of FA in the solutions obtained from the molality and density data (see Section 2.2). Eqn (9) is a simplified form of the Jones–Dole equation reported in the literature:[36]

$$\eta_r = \frac{\eta}{\eta_0} = 1 + Ac^{1/2} + Bc \quad (10)$$

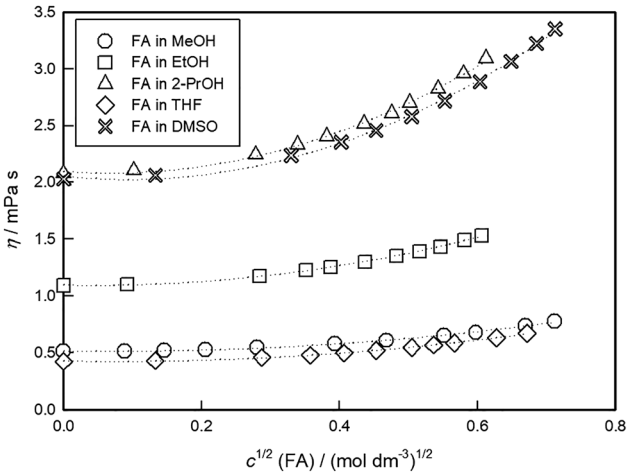

Fig. 2 Concentration dependence of viscosity, η, for FA in the investigated solvents at a temperature of 298.15 K.

The viscosity *B*-coefficient measures ion–solvent interactions, *i.e.* the association of solvent molecules with the ion (solvation), while the *A*-coefficient measures ion–ion interactions. In this case, the *B*-coefficient is significantly bigger than the *A*-coefficient; this was proven by processing viscometric data using eqn (10) in our work, *e.g.* for FA in MeOH at 298.15 K. For that reason, in the present study eqn (10) was applied. The same equation was used in the literature to calculate the *B*-coefficients of nicotinic acid in an aqueous solution of D-xylose/L-arabinose at different temperatures.[48] Our obtained values for *B*-coefficients in different solvents for different temperatures are listed in Table 1.

The Jones–Dole viscosity *B*-coefficients for FA are positive across all studied solvents and in the entire temperature range. This indicates strong solute–solvent interactions in both protic and aprotic solvents. In methanol, ethanol, THF, and DMSO, the *B*-coefficient decreases with increasing temperature, while the *B*-coefficients obtained in 2-propanol display non-monotonic temperature dependence and significantly larger scatter, especially at intermediate temperatures. If 2-PrOH is excluded from Table 1, then it can be seen that coefficient *B* is higher in polar aprotic solvents (THF or DMSO) than polar aprotic solvents (MeOH or EtOH). So, it follows that ion–solvent interactions are stronger in these solvents, compared to protic ones.

From the data given in Table 1, the *B*-coefficients mostly decrease with increasing temperature in a particular solvent. At a given temperature, $T = 298.15$ K, the value of the *B*-coefficient for FA is the highest in THF. In this work, using SigmaPlot 10.0, regression analysis of the data $B = f(T)$ was performed. The result of processing are polynomial functions of the second order:

$$B(\text{FA–MeOH}) = 4.9897 - 0.0197T + 2.1212 \times 10^{-5}T^2, \quad (11)$$

$$B(\text{FA–EtOH}) = 5.6880 - 0.0211T + 1.8881 \times 10^{-5}T^2, \quad (12)$$

$$B(\text{FA–2-PrOH}) = 30.2264 - 0.1883T + 3 \times 10^{-4}T^2, \quad (13)$$

$$B(\text{FA–THF}) = 13.7539 - 0.0773T + 1 \times 10^{-4}T^2, \quad (14)$$

$$B(\text{FA–DMSO}) = 5.3253 - 0.0178T + 1.4286 \times 10^{-5}T^2. \quad (15)$$

The analysis of the sign of the viscosity coefficient *B* derivative in relation to temperature (dB/dT) for FA in the investigated solvents provides significant information about the role of the solute being either constructive or destructive for the solvent structure. According to established criteria from the literature,[49,50] negative values of dB/dT indicate structure-making behavior, while positive values correspond to structure-breaking. The temperature coefficient, dB/dT in $dm^3\ mol^{-1}\ K^{-1}$, which is derived from the above eqn, at 298.15 K, is: -7.1×10^{-3} (FA–MeOH), -9.8×10^{-3} (FA–EtOH), -9.4×10^{-3} (FA–2-PrOH), -1.8×10^{-2} (FA–THF), and -9.3×10^{-3} (FA–DMSO). It is evident that the viscosity *B*-coefficients for all tested systems show the trend of a decrease with the temperature which can be attributed to the structure making nature of FA. Viscosity measurements carried out by Chen *et al.* for FA in aqueous ethanol or 1-propanol solutions at various temperatures showed that the viscosity *B*-coefficients are positive and decrease with the increase in temperature. As in our work, their negative dB/dT values of FA indicate that FA acts as a structure-maker solute in investigated systems.[39]

Additionally, an illustration of the Jones–Dole plot for a selected system (FA–DMSO) at different temperatures is given in Fig. 3. The plot of $(\eta_r - 1)$ *vs.* c (rearranged Jones–Dole eqn (9)) for all working temperatures, is presented as an example. The viscosity *B*-coefficients were estimated from the slopes of the curves, using the SigmaPlot 10.0 graphical tool. Linear fits were obtained for the other tested systems with high correlation coefficient, $R \geq 0.99$.

3.2 Simulation results

3.2.1 Shear viscosity results. The calculated shear viscosities are presented in Table 2. The shear viscosity results obtained from the simulations show a reasonable agreement with the measurements, given that the utilized force fields were not parametrized to reproduce shear viscosity. While the experiments show a clear trend of viscosity increasing with an increase of the molar fraction of FA and a decrease in temperature, the simulation results are not so consistent for all the solvents. However, the calculated values show solid quantitative alignment to the experimental results, thus encouraging us to analyze the microstructure of these mixtures.

Table 1 Viscosity *B*-coefficients for ferulic acid (FA) in different solvents at different temperatures[a]

T/K	MeOH	EtOH	2-PrOH	THF	DMSO
273.15	1.159 ± 0.028	1.335 ± 0.029	1.539 ± 0.049	1.511 ± 0.046	—
278.15	1.166 ± 0.030	1.287 ± 0.026	1.484 ± 0.042	1.466 ± 0.044	—
283.15	1.119 ± 0.029	1.229 ± 0.025	1.472 ± 0.052	1.412 ± 0.043	—
288.15	1.082 ± 0.028	1.174 ± 0.023	1.378 ± 0.045	1.365 ± 0.042	—
293.15	1.026 ± 0.026	1.128 ± 0.021	1.367 ± 0.050	1.327 ± 0.039	1.322 ± 0.043
298.15	1.007 ± 0.022	1.083 ± 0.019	1.276 ± 0.037	1.292 ± 0.036	1.278 ± 0.041
303.15	0.983 ± 0.026	1.043 ± 0.019	1.125 ± 0.018	1.257 ± 0.035	1.227 ± 0.038
308.15	0.945 ± 0.024	1.021 ± 0.019	1.158 ± 0.024	1.229 ± 0.035	1.185 ± 0.037
313.15	0.925 ± 0.023	0.886 ± 0.029	1.605 ± 0.090	1.214 ± 0.035	1.139 ± 0.041
318.15	0.873 ± 0.019	0.867 ± 0.040	1.245 ± 0.030	1.206 ± 0.034	1.095 ± 0.039
323.15	0.840 ± 0.018	0.874 ± 0.054	1.347 ± 0.046	1.215 ± 0.035	1.347 ± 0.029

[a] Unit: *B*, $dm^3\ mol^{-1}$.

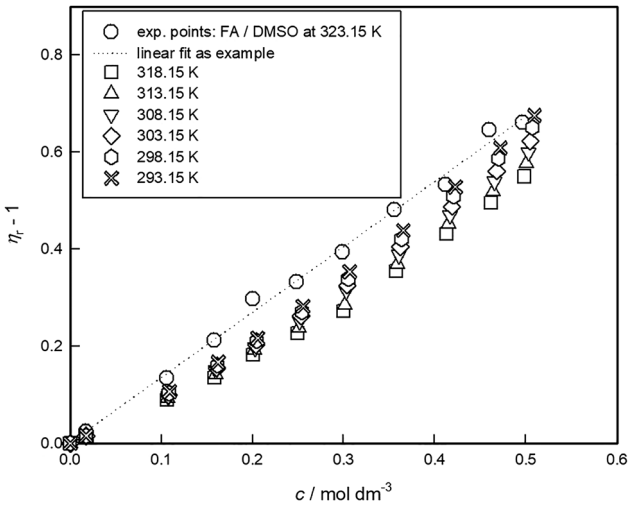

Fig. 3 Jones–Dole plot for FA in DMSO as an example at different temperatures.

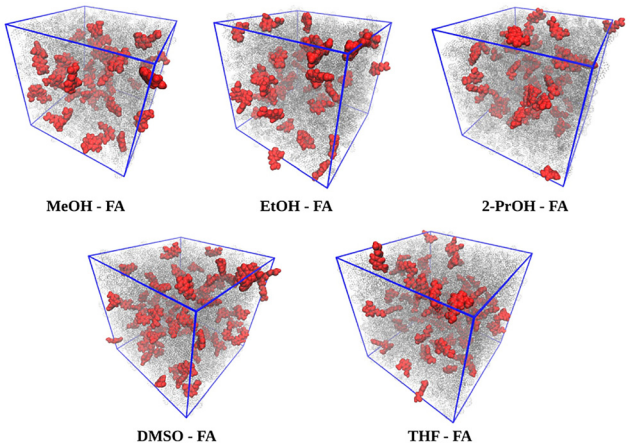

Fig. 4 Snapshots of the MeOH–FA system (top left), EtOH–FA (top center), 2PrOH–FA (top right), DMSO–FA system (bottom left) and THF–FA system (bottom right) for the highest mole fraction of FA and at T = 298 K. The FA molecules are shown explicitly in the VdW representation (red), while the solvent is depicted in the eponymous representation (gray). All visualizations were made using the VMD program.[51]

Table 2 The shear viscosity η, calculated from simulations for five binary mixture systems, with two mole fractions of FA for each system at three temperatures

η/mPa s	278 K	298 K	318 K
MeOH–FA			
x(FA) = 0.01274	0.82 ± 0.05	0.96 ± 0.07	0.51 ± 0.02
x(FA) = 0.02169	2.12 ± 0.12	0.99 ± 0.04	0.35 ± 0.03
EtOH–FA			
x(FA) = 0.01134	0.48 ± 0.08	0.61 ± 0.04	0.73 ± 0.05
x(FA) = 0.0221	2.66 ± 0.16	0.56 ± 0.05	1.04 ± 0.13
2-PrOH–FA			
x(FA) = 0.01474	3.55 ± 0.25	1.68 ± 0.16	2.00 ± 0.20
x(FA) = 0.02943	3.67 ± 0.32	1.65 ± 0.11	0.39 ± 0.05
DMSO–FA			
x(FA) = 0.01849	1.38 ± 0.12	1.50 ± 0.11	0.96 ± 0.06
x(FA) = 0.03761	1.72 ± 0.13	1.12 ± 0.11	1.39 ± 0.06
THF–FA			
x(FA) = 0.01698	0.38 ± 0.04	0.20 ± 0.02	0.51 ± 0.03
x(FA) = 0.03778	0.58 ± 0.03	0.48 ± 0.02	0.70 ± 0.04

3.2.2 Structural properties. Fig. 4 shows the simulation boxes for all five systems at the temperature T = 298 K and at the highest simulated FA mole fractions. The molecules of FA are depicted in red, whereas the solvents are represented in "solvent" mode in gray. A casual glance reveals that FA molecules are dispersed in each solvent, exhibiting no aggregation amongst themselves. Therefore, it becomes instructive to examine the structural properties of the pairs of atoms in the solvent and also the cross pairs between the solvent and FA, rather than the pairs of atoms in FA itself.

We present further results for the binary mixtures of FA with one representative of the protic solvents, 2-propanol, and one representative of the aprotic solvents, DMSO, since the general trends between the two solvent groups are the same.

Fig. 5 contains the pair correlation functions for the oxygen sites in 2-propanol (left panel) and the cross correlations between the oxygen in 2-propanol with the oxygen site O3 in FA (middle panel) and oxygen site O4 in FA (right panel), respectively. Due to the small number of molecules of FA, the $g(r)$ for the O3–O3 and O4–O4 correlations are too noisy to provide relevant information. However, the pair correlation functions presented in Fig. 5 provide ample evidence of hydrogen bonding. The sharp and narrow first peak, typical of hydrogen bonding,[52,53] is present in all OO correlations and indicative of structure-making. Since 2-propanol is in the majority, its OO correlations are systematically the highest, followed by the cross O–O3 correlations and then cross O–O4 correlations. The difference in the peak heights for the cross correlations stems from the different positions of the two OH groups in FA (Fig. 6), where the O4 hydroxyl group is attached to the bulky ring, thus being less accessible for hydrogen bonding. The effect of FA mole fraction is the same over all OO correlations, with both mole fractions of FA yielding the same correlations for all temperatures. With the increase in temperature, there is a decrease in the first neighbour correlations for all combinations. These trends are the same for the other protic, hydrogen bonding solvents, methanol and ethanol, whose corresponding pair correlation functions can be found in Fig. S2 and S3 in the SI.

The pair correlation functions for the oxygen sites in DMSO (left panel) and the cross correlations between the oxygen in DMSO with the oxygen site O3 in FA (middle panel) and oxygen site O4 in FA (right panel) are shown in Fig. 7. Since DMSO doesn't form hydrogen bonds with itself, its OO correlation functions behave like that of a simple liquid, *i.e.* with a broad first peak that doesn't vary with the change in mole fraction of FA or temperature. The cross correlations, especially that of O–O3, reveal a different story as the tall, sharp and narrow first

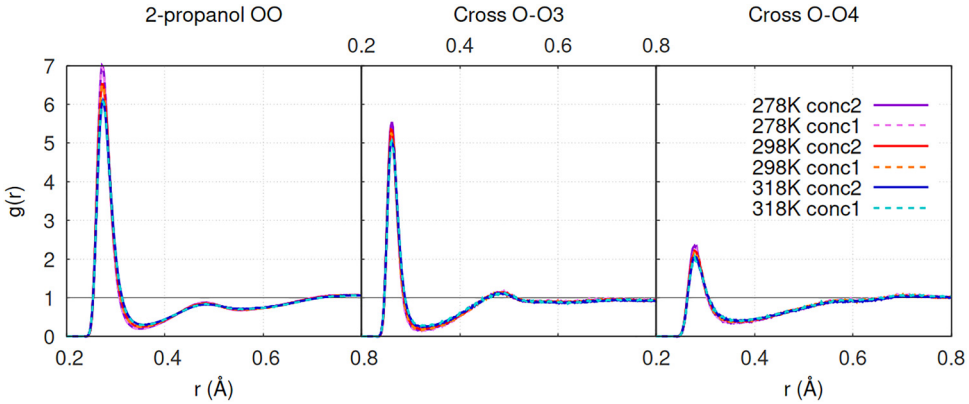

Fig. 5 The pair correlation functions for the OO sites in: 2-propanol (left), 2-propanol O–FA O3 (center) and 2-propanol O–FA O4 (right), for 3 temperatures (278 K – purple tones, 298 K – red tones, 318 K – blue tones) and 2 mole fractions (x(FA) = 0.01474 as conc1 and x(FA) = 0.02943 as conc2).

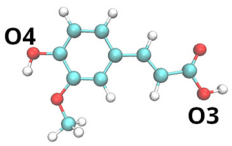

Fig. 6 The graphical depiction of the FA molecule, with the O3 and O4 sites marked.

peak indicates hydrogen bonding, thus giving a persuasive argument towards structure-making. The O–O4 correlations also result in a sharp and narrow first peak, but it's depleted due to the steric effects imposed by the ring that particular OH group is attached to (Fig. 6). The general trends observed for the DMSO–FA system are valid for the THF–FA system (Fig. S4 in the SI).

The coordination numbers corresponding to first neighbors from the pair correlations in Fig. 5 and 7 are given in Table 3. The coordination number of OO in 2-propanol in its bulk state revolves around 2, given that the hydroxyl groups in neat monools form chains which have 2 neighbors.[54] The trends for OO in 2-propanol exhibit a decrease in the coordination number with an increase in temperature and an increase in the FA content. Conversely, the coordination numbers for the cross varieties increase with the added FA molecules. Even though the small mole fractions of FA yield numerically small coordination numbers, there is a clear pattern of an increase in first neighbors between cross species and a decrease in the first neighbors of 2-propanol, which is another argument in favor of structure-making. A similar trend is observed for the coordination numbers for the case of DMSO–FA, though it is important to note that the number of first neighbors for O atoms in DMSO is around 12, which is a hallmark of a simple liquid.[55]

The coordination numbers for the first neighbors for the three other systems are available in the SI, Table S6, and follow the described trends.

The cluster probability distributions in Fig. 8 are calculated for the oxygen sites in 2-propanol (left panel) and all the oxygen sites in the system, both in 2-propanol and in FA (right panel). The cluster distributions in 2-propanol have the same features as those in neat alcohols,[56,57] the most prominent of which is the peak occurring at 4–6 member clusters, indicating the highest probability for clusters of those particular sizes. This

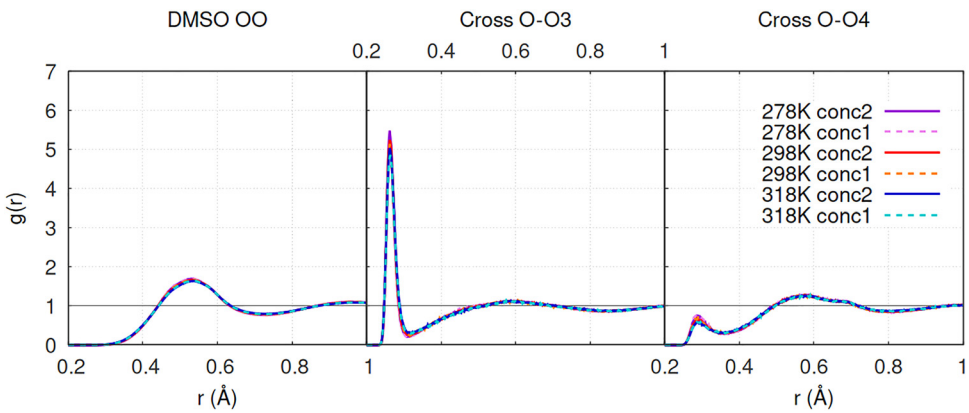

Fig. 7 The pair correlation functions for the OO sites in: DMSO (left), DMSO O – FA O4 (center) and 2-propanol O – FA O3 (right), for 3 temperatures (278 K – purple tones, 298 K – red tones, 318 K – blue tones) and 2 mole fractions (x(FA) = 0.01849 as conc1 and x(FA) = 0.03761 as conc2).

Table 3 Coordination numbers for the first neighbors in 2-PrOH–FA and DMSO–FA, calculated from the pair correlation functions in Fig. 5 and 7

	278 K			298 K			318 K		
$n(r)$	OO	O3O	O4O	OO	O3O	O4O	OO	O3O	O4O
2-PrOH–FA									
x(FA) = 0.01474	1.964	0.016	0.013	1.963	0.016	0.013	1.939	0.017	0.013
x(FA) = 0.02943	1.918	0.032	0.028	1.902	0.032	0.027	1.883	0.033	0.027
DMSO–FA									
x(FA) = 0.01849	12.464	0.021	0.008	12.013	0.020	0.007	11.970	0.020	0.007
x(FA) = 0.03761	11.367	0.039	0.016	11.327	0.040	0.014	11.272	0.041	0.013

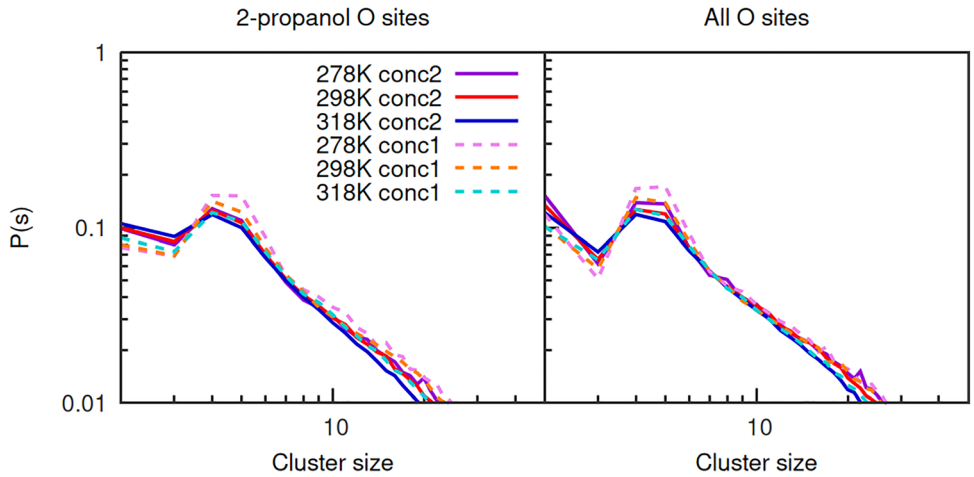

Fig. 8 The cluster distribution probabilities for O sites in 2-propanol (left panel) and all O sites in the binary mixture (right panel) for 3 temperatures (278 K – purple tones, 298 K – red tones, 318 K – blue tones) and 2 mole fractions (x(FA) = 0.01474 as conc1 and x(FA) = 0.02943 as conc2).

feature is present for all 3 temperatures and both mole fractions, though there seems to be a slight increase for the smaller mole fraction at 278 K (light purple dashed line). When we consider all O atoms in the system, it is clear that the distributions retain the same general trend, with the cluster peak at 4–6 clusters having an even bigger probability for all temperatures and mole fractions. Additionally, the distributions for all O sites shift towards larger cluster sizes as compared to those of only O sites in 2-propanol. Both of these features point to the structure-making properties of FA. The same pattern is present in the binary mixtures of FA with methanol and ethanol, respectively, as can be seen in Fig. S5 and S6 in the SI.

3.2.2.1 Hydrogen bonding. In the case of protic solvents, it is interesting to analyze the hydrogen bonding, the signatures of which are prominently featured in the pair correlation

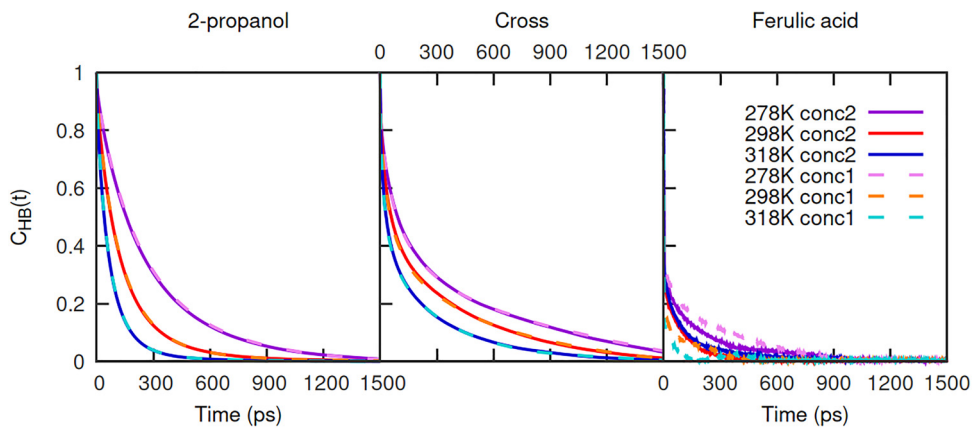

Fig. 9 The continuous hydrogen bond autocorrelation functions C(t) for: 2-propanol (left), 2-propanol–FA (center) and FA (right), for 3 temperatures (278 K – purple tones, 298 K – red tones, 318 K – blue tones) and 2 mole fractions (x(FA) = 0.01474 as conc1 and x(FA) = 0.02943 as conc2).

Table 4 Continuous hydrogen-bond lifetimes τ_{HB}^{cont} calculated from the autocorrelation function in Fig. 9 for the 2-PrOH–FA binary mixture

	278 K			298 K			318 K		
τ_{HB}^{cont} [ps]	2-PrOH	Cross	FA	2-PrOH	Cross	FA	2-PrOH	Cross	FA
2-PrOH–FA									
x(FA) = 0.01474	265.4	281.8	87.1	139.1	210.8	24.9	76.1	139.5	13.1
x(FA) = 0.02943	259.3	280.2	65.6	137.9	212.2	30.6	75.1	141.0	43.6

functions and cluster distribution probabilities. Fig. 9 contains the continuous hydrogen bond autocorrelation functions in the 2-propanol–FA system. Out of all three species combinations, the hydrogen bonds between FA and 2-propanol decay the slowest for all three temperatures, once again supporting the idea of FA being the structure maker. The mole fraction of FA plays no role for the cross $C_{HB}(t)$, but the temperature does – the $C_{HB}(t)$ decay faster with an increase in temperature. These observations hold true for the hydrogen bonds between 2-propanol, which decay faster than those between cross species. The hydrogen bonds between FA decay the most rapidly, especially as the temperature increases. There is variation with the mole fraction, but this might be due to the statistics being done on a small sample.

These patterns are numerically confirmed if we examine Table 4, which contains the continuous hydrogen-bond lifetimes τ_{HB}^{cont}. The $C_{HB}(t)$ functions and τ_{HB}^{cont} lifetimes for methanol–FA and ethanol–FA, presented in the Supplementary information (Fig. S7, S8 and Table S7), corroborate these findings and confirm the structure-making role of FA.

The structure-making argument is strengthened when we examine the intermittent hydrogen bond autocorrelation functions and its corresponding intermittent hydrogen-bond lifetimes. The observations for $C(t)$ and τ_{HB}^{cont} apply to the case of $H(t)$ and τ_{HB}^{int} as well. The intermittent hydrogen bonds between FA and the alcohol decay the slowest, followed by those between 2-propanol and then those with FA (Fig. 10), which is supported by the corresponding intermittent hydrogen bond lifetimes listed in Table 5. The same is true for the mixtures of methanol–FA and ethanol–FA, the intermittent hydrogen bond data of which are presented in the SI (Fig. S9, S10 and Table S8).

3.2.2.2 Antioxidant capacity of ferulic acid. The antioxidant capacity of FA in selected solvents was evaluated using the DPPH radical scavenging assay and the FRAP reducing power assay. These assays have different mechanisms of action. The DPPH assay tests the ability of a compound to donate electrons or hydrogen atoms to neutralize free radicals. This is done through the DPPH radical, which is reduced when it reacts with an antioxidant, such as FA. The IC_{50} value, in this case, represents the concentration of FA required to reduce 50% of the DPPH radicals. It is inversely related to antioxidant potency, so the lower IC_{50} value indicates stronger radical-scavenging activity. FRAP, on the other hand, measures the ability of a

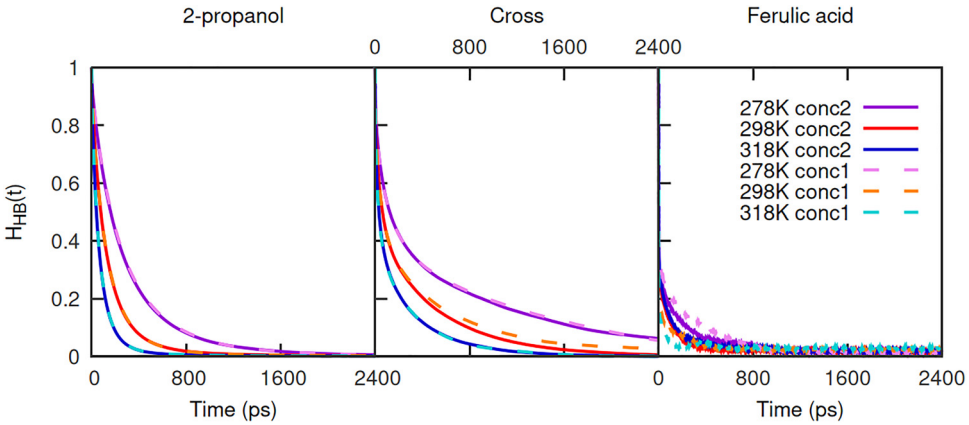

Fig. 10 The intermittent hydrogen bond autocorrelation functions $H(t)$ for: 2-propanol (left), 2-propanol–FA (center) and FA (right), for 3 temperatures (278 K – purple tones, 298 K – red tones, 318 K – blue tones) and 2 mole fractions (x(FA) = 0.01474 as conc1 and x(FA) = 0.02943 as conc2).

Table 5 Intermittent hydrogen-bond lifetimes τ_{HB}^{int} calculated from the autocorrelation function in Fig. 10 for the 2-PrOH–FA binary mixture

	278 K			298 K			318 K		
τ_{HB}^{int} [ps]	2-PrOH	Cross	FA	2-PrOH	Cross	FA	2-PrOH	Cross	FA
2-PrOH–FA									
x(FA) = 0.01474	294.1	498.6	122.8	146.0	297.5	79.7	79.1	148.6	81.5
x(FA) = 0.02943	287.8	487.6	104.7	145.2	250.6	74.7	78.4	150.3	89.1

Table 6 The antioxidant capacity of FA in selected solvents, obtained by the DPPH and FRAP methods. IC_{50} was determined from the curve plotting the concentration of the tested sample against the percentage of DPPH inhibition

	DPPH IC_{50} mmol L^{-1}	FRAP mmol L^{-1} Fe^{2+}
FA/EtOH	0.82	1938
FA/MetOH	0.15	1350
FA/THF	0.37	1944
FA/DMSO	0.47	2494

compound to reduce Fe^{3+} to Fe^{2+}. The higher the Fe^{2+} concentration, the greater the reducing ability of the compound.

The antioxidant capacity of FA in selected solvents, obtained by both methods, is summarized in Table 6. In the DPPH assay, the lowest IC_{50} value was obtained for FA dissolved in methanol (0.15 mM), followed by FA in tetrahydrofuran (0.37 mM) and DMSO (0.47 mM), whereas the highest IC_{50} was observed for FA in ethanol (0.82 mM). In the FRAP assay, the highest reducing capacity was observed for FA in DMSO (2494 mmol L^{-1} Fe^{2+}), followed by FA in THF (1944 mmol L^{-1} Fe^{2+}) and FA in ethanol (1938 mmol L^{-1} Fe^{2+}), while the lowest value was obtained for FA in methanol (1350 mmol L^{-1} Fe^{2+}).

The obtained results show that the DPPH and FRAP methods do not necessarily yield the same activity trend. For example, FA in methanol exhibited the lowest IC_{50} value in the DPPH assay, but it also showed the weakest reducing capacity in the FRAP assay. On the other hand, FA in DMSO displayed the highest reducing capacity in the FRAP assay but had a relatively higher IC_{50} value in the DPPH assay.

These differences can be connected to several factors, the first of which is the distinct reaction mechanism of the two assays – DPPH's free-radical scavenging ability *versus* the reducing power in FRAP. The second factor is the choice of solvent. The physico-chemical and solvation properties of the solvent, its microstructure and the solvent's interaction with the FA molecule can influence its antioxidant activity. FA performs differently in different solvents, depending on the type of antioxidant action being measured, but it is important to note that FA exhibits antioxidant activity in both assays. The two methods are complementary and together provide a more comprehensive picture of the antioxidant profile of FA.

The present results suggest that the basic radical-scavenging and reducing functionality of FA is largely preserved upon changing the solvent. This observation is consistent with the picture emerging from viscosity experiments and MD simulations, where FA acts as a structure-making solute that organizes its solvation shell and engages in persistent hydrogen bonding with protic solvents. In such a structured environment, the phenolic OH groups of FA are expected to remain accessible for radical-scavenging or electron-transfer reactions across different media, although subtle solvent effects can modulate the relative responses in the DPPH and FRAP assays.

Ethanol deserves particular attention because it combines appreciable antioxidant responses in both assays with a favourable toxicological and technological profile, and FA is poorly soluble in water. FA–ethanol solutions are therefore attractive for potential pharmaceutical or cosmetic formulations.

4. Conclusions

The merits of FA as an antioxidant with potential for various medical applications have been widely discussed in the literature. The present study adds to that body of knowledge by investigating the molecular interactions and structuring in binary mixtures of FA with five different solvents *via* viscosity experiments and molecular dynamic simulations. Viscosity measurements for FA in methanol, ethanol, 2-propanol, tetrahydrofuran and dimethyl sulfoxide have provided precise reference data across a range of temperatures and mole fractions of FA, revealing that the Jones–Dole *B* parameters are positive in all systems and that their temperature derivatives are negative. This points to the fact that FA acts like a structure maker in all of the tested solvents. This was further corroborated by simulations, where all of the calculated quantities witnessed signatures of structure-making. In terms of the local structure, there were appreciable correlations between cross-species for all of the simulated mixtures. In the protic solvents, the cluster probability distributions showed prominent signatures of clustering that involved both FA and the solvent. This was further underscored with the hydrogen bond analysis, where in each mixture of FA and protic solvents the cross species hydrogen bonds were the longest lasting, regardless of being continuous or intermittent hydrogen bonds. Finally, the measurement of the antioxidant capacity of FA in selected solvents revealed highly promising antioxidant potential. This hints at the fact that FA can impose a certain type of structuring regardless of the solvent, and that in turn supports antioxidant reactivity in all solvents. Taken together, the viscosity analysis, molecular simulations and antioxidant tests provide a consistent picture in which ferulic acid acts as a structure-making solute that reorganizes the neat solvent into a more ordered solvation environment while preserving its antioxidant activity across different organic solvents.

Author contributions

Renato Tomaš: conceptualization, methodology, investigation (density and viscosity measurements), formal analysis, validation, writing – original draft, funding acquisition, writing – review & editing. Olivera Politeo: methodology, investigation (biochemical analysis of ferulic acid), formal analysis, writing – original draft, writing – review & editing Milan Vraneš: software, supervision, writing – review & editing. Moez Guettari: visualization, figure generation, supervision, writing – review & editing. Safija Herenda: table generation, searching and analyzing literary sources, project administration, writing – review & editing. Martina Požar: conceptualization, methodology, investigation (molecular dynamics simulations), formal analysis, validation, writing – original draft, writing – review & editing,

correspondence. All authors read and approved the final manuscript.

Conflicts of interest

The authors declare that they have no known competing financial interests or personal relationships that could have appeared to influence the work reported in this paper.

Data availability

The density and viscosity measurements generated in this study are provided in the supplementary information (SI). The simulation outputs, including calculated viscosity data, pair correlation functions, cluster distributions, and hydrogen-bond analyses, are presented in the manuscript and in the supplementary information. The molecular-dynamics simulation input files and full trajectory data can be made available by the corresponding author upon reasonable request. Supplementary information is available. See DOI: https://doi.org/10.1039/d5cp04726a.

Acknowledgements

This work was financially supported by the Faculty of Chemistry and Technology, University of Split through the institutional project ''Molecular interactions in the system electrolyte or nonelectrolyte–solvent: thermodynamic and transport properties''.

References

1 M. A. Alam, N. Subhan, H. Hossain, M. Hossain, H. M. Reza, M. M. Rahman and M. O. Ullah, *Nutr. Metab.*, 2016, **13**, 27.
2 M. Iranshahy and M. Iranshahi, *J. Ethnopharmacol.*, 2011, **134**, 1–10.
3 X. Zhang, B. Han, Z.-M. Feng, Y.-N. Yang, J.-S. Jiang and P.-C. Zhang, *Fitoterapia*, 2018, **125**, 147–154.
4 C. Andrs-Lacueva, A. Medina-Remon, R. Llorach, M. Urpi-Sarda, N. Khan, G. Chiva-Blanch, R. Zamora-Ros, M. Rotches-Ribalta and R. M. Lamuela-Ravents, *Fruit and Vegetable Phytochemicals*, Wiley-Blackwell, Oxford, UK, 2009, pp. 53–88.
5 E. Kilinc and H. Kalkan, *J. Wine Res.*, 2003, **14**, 17–23.
6 D. Li, Y.-X. Rui, S.-D. Guo, F. Luan, R. Liu and N. Zeng, *Life Sci.*, 2021, **284**, 119921.
7 D. D. Peres, F. D. Sarruf, C. A. de Oliveira, M. V. R. Velasco and A. R. Baby, *J. Photochem. Photobiol., B*, 2018, **185**, 46–49.
8 H.-J. Park, J.-H. Cho, S.-H. Hong, D.-H. Kim, H.-Y. Jung, I.-K. Kang and Y.-J. Cho, *J. Nat. Med.*, 2018, **72**, 127–135.
9 J. Gao, H. Yu, W. Guo, Y. Kong, L. Gu, Q. Li, S. Yang, Y. Zhang and Y. Wang, *Cancer Cell Int.*, 2018, **18**, 102.
10 U. Sherefedin, A. Belay, K. Gudishe, A. Kebede, A. G. Kumela, T. Feyisa, J. H. Mahamud and S. Fekadu, *Results Chem.*, 2025, **13**, 101996.
11 A. Narasimhan, M. Chinnaiyan and B. Karundevi, *Appl. Physiol., Nutr., Metab.*, 2015, **40**, 769–781.
12 E. M. Neto-Neves, C. da Silva Maia Bezerra Filho, N. N. Dejani and D. P. de Sousa, *Mini-Rev. Med. Chem.*, 2021, **21**, 1625–1637.
13 R. Sultana, *Biochim. Biophys. Acta*, 2012, **1822**, 748–752.
14 S. Ojha, H. Javed, S. Azimullah, S. B. Abul Khair and M. E. Haque, *Drug Des., Dev. Ther.*, 2015, **9**, 5499–5510.
15 W. Song, J. Xin, C. Yu, C. Xia and Y. Pan, *Front. Microbiol.*, 2023, **14**, 1135308.
16 F. Shakeel, M. M. Salem-Bekhit, N. Haq and N. A. Siddiqui, *J. Mol. Liq.*, 2017, **236**, 144–150.
17 B. Chen, K. Liu, L. Wang, X. Zhang, K. Qu, Y. Kong and M. Liu, *J. Chem. Eng. Data*, 2022, **67**, 3414–3425.
18 M. Sahin, N. Erkan and E. Ayranci, *J. Solution Chem.*, 2016, **45**, 52–66.
19 D. Villanueva-Bermejo, G. Reglero, R. P. Stateva and T. Fornari, *Open Chem. Eng. J.*, 2016, **10**, 50–58.
20 T. Lin, Q. Zhang, R. Liang and X. Zhang, *Ind. Eng. Chem. Res.*, 2024, **63**, 4113–4123.
21 L. Chen, M. Zhu, X. Hu, J. Pan and G. Zhang, *J. Sci. Food Agric.*, 2022, **102**, 3835–3846.
22 B. L. Amshumala, G. Pavan, K. P. Sharmila, N. Suchetha Kumari and G. Tamizh Selvan, *J. Mol. Liq.*, 2024, 126703.
23 Y. Yang, S. Wang, X. Liu, W. Zhang, W. Tong, H. Luo and L. Zhao, *Heliyon*, 2024, **10**, e24605.
24 I. Antonopoulou, E. Sapountzaki, U. Rova and P. Christakopoulos, *Biomedicines*, 2022, **10**, 1787.
25 R. L. Prior, X. Wu and K. Schaich, *J. Agric. Food Chem.*, 2005, **53**, 4290–4302.
26 I. G. Munteanu and C. Apetrei, *Int. J. Mol. Sci.*, 2021, **22**, 3380.
27 M. Olszowy-Tomczyk, *Chem. Pap.*, 2021, **75**, 6157–6167.
28 F. Xiao, T. Xu, B. Lu and R. Liu, *Food Front.*, 2020, **1**, 60–69.
29 Z. Kinart and R. Tomaš, *Int. J. Electrochem. Sci.*, 2020, **15**, 5560–5570.
30 R. Tomaš, M. Vraneš, A. Krešo, Z. Kinart, T. T. Borović and S. Papović, *J. Solution Chem.*, 2023, **52**, 134–146.
31 DIN 51757 (0.41994) Testing of mineral oils and related materials – determination of density. 2011. Available: https://www.document-center.com/standards/show/DIN-51757.
32 W. Brand-Williams, M. E. Cuvelier and C. Berset, *Lebenson. Wiss. Technol.*, 1995, **28**, 25–30.
33 I. F. Benzie and J. J. Strain, *Anal. Biochem.*, 1996, **239**, 70–76.
34 M. J. Abraham, T. Murtola, R. Schulz, S. Páll, J. C. Smith, B. Hess and E. Lindahl, *SoftwareX*, 2015, **1–2**, 19–25.
35 W. L. Jorgensen, *J. Phys. Chem.*, 1986, **90**, 1276–1284.
36 J. M. Briggs, T. Matsui and W. L. Jorgensen, *J. Comput. Chem.*, 1990, **11**, 958–971.
37 W. L. Jorgensen, D. S. Maxwell and J. Tirado-Rives, *J. Am. Chem. Soc.*, 1996, **118**, 11225–11236.
38 L. Martínez, R. Andrade, E. G. Birgin and J. M. Martínez, *J. Comput. Chem.*, 2009, **30**, 2157–2164.
39 G. Bussi, D. Donadio and M. Parrinello, *J. Chem. Phys.*, 2007, **126**, 014101.

40 M. Parrinello and A. Rahman, *Phys. Rev. Lett.*, 1980, **45**, 1196–1199.
41 M. Parrinello and A. Rahman, *J. Appl. Phys.*, 1981, **52**, 7182–7190.
42 R. Hockney, *Methods in computational physics*, Orlando Academic Press, 1970, vol. 9, pp. 135–221.
43 T. Darden, D. York and L. Pedersen, *J. Chem. Phys.*, 1993, **98**, 10089–10092.
44 B. Hess, H. Bekker, H. J. C. Berendsen and J. G. E. M. Fraaije, *J. Comput. Chem.*, 1997, **18**, 1463–1472.
45 J.-P. Hansen and I. R. McDonald, *Theory of Simple Liquids*, Elsevier, 2006.
46 A. Luzar and D. Chandler, *Nature*, 1996, **379**, 55–57.
47 A. Luzar, *J. Chem. Phys.*, 2000, **113**, 10663–10675.
48 B. Chen, K. Liu, D. Wang, Y. Kong, K. Qu, X. Zhang and M. Liu, *J. Chem. Eng. Data*, 2022, **67**, 1089–1100.
49 H. D. B. Jenkins and Y. Marcus, *Chem. Rev.*, 1995, **95**, 2695–2724.
50 M. Kaminsky, *Discuss. Faraday Soc.*, 1957, **24**, 171.
51 W. Humphrey, A. Dalke and K. Schulten, *J. Mol. Graphics*, 1996, **14**(33–38), 27–28.
52 M. Požar, J.-B. Seguier, J. Guerche, R. Mazighi, L. Zoranić, M. Mijaković, B. Kežić-Lovrinčević, F. Sokolić and A. Perera, *Phys. Chem. Chem. Phys.*, 2015, **17**, 9885–9898.
53 M. Požar, B. Lovrinčević, L. Zoranić, T. Primorać, F. Sokolić and A. Perera, *Phys. Chem. Chem. Phys.*, 2016, **18**, 23971–23979.
54 M. Požar and A. Perera, *Chem. Phys. Lett.*, 2017, **671**, 37–43.
55 H. Jónsson and H. C. Andersen, *Phys. Rev. Lett.*, 1988, **60**, 2295–2298.
56 A. Perera, F. Sokolić and L. Zoranić, *Phys. Rev. E: Stat., Nonlinear, Soft Matter Phys.*, 2007, **75**, 060502.
57 L. Zoranić, F. Sokolić and A. Perera, *J. Chem. Phys.*, 2007, **127**, 024502.